Available online at www.sciencedirect.com
ScienceDirect
Journal of Power Sources 168 (2007) 338–345
JOURNAL OF POWER SOURCES
www.elsevier.com/locate/jpowsour

Characterization of electrical properties of GDC doped A-site deficient LSCF based composite cathode using impedance spectroscopy

Fu Qiang [a], KeNing Sun [a,*], NaiQing Zhang [a,b], XiaoDong Zhu [a], ShiRu Le [a], DeRui Zhou [a]

[a] *Department of Applied Chemistry, Harbin Institute of Technology, Harbin 150001, China*
[b] *The Research Station on Material Science and Engineering for Postoral Fellows, Harbin Institute of Technology, Harbin 150001, China*

Received 3 February 2007; received in revised form 15 March 2007; accepted 15 March 2007
Available online 24 March 2007

Abstract

The composite cathode consisting of A-site deficient perosvkite material $La_{0.58}Sr_{0.4}Co_{0.2}Fe_{0.8}O_{3-\delta}$ (L58SCF) and $Ce_{0.8}Gd_{0.2}O_{2-\delta}$ (GDC) on YSZ electrolyte is studied for potential applications in intermediate/low-temperature solid oxide fuel cells (SOFCs). Impedance spectroscopy measurements are performed in air over the temperature range of 600–800 °C under open circuit potential. The results show that the addition of 40 wt.% GDC to L58SCF (L58SCF–GDC40) results in the lower polarization resistance (0.07 Ω cm^2 at 800 °C, 0.11 Ω cm^2 at 750 °C and 0.22 Ω cm^2 at 700 °C) than other composite cathodes and its activation energy values calculated for the low- and high-frequency arcs are 0.86 and 1.10 eV, respectively. The composite cathode exhibit high exchange current density and low charge-transfer resistance.

Keywords: SOFC; Composite cathode; Impedance; Perosvkite; Polarization

1. Introduction

The perovskite material $La_{0.6}Sr_{0.4}Co_{0.2}Fe_{0.8}O_{3-\delta}$ (LSCF) is one of the more promising cathode materials for SOFC operation below 800 °C. It is known that oxygen ionic conductivity is attributed to the concentration of oxygen carrier—oxygen vacancy. The oxide ion conductivity can be increased by the creation of more oxygen vacancies [1,2]. A-site deficient perosvkite material $La_{0.58}Sr_{0.4}Co_{0.2}Fe_{0.8}O_{3-\delta}$ (L58SCF) increases the ionic and electronic conductivity and the surface exchange of oxygen, which can be explained by the larger number of oxygen vacancies and electronic holes [6]. It was reported that the measured current densities of cells with A site deficient cathodeL58SCF, were as high as 1.76 A cm^{-2} at 800 °C and 0.7 V, which is about twice the current density of cells with (La, Sr)MnO_3/yttrium-stabilized zirconia (LSM/YSZ) composite cathodes [6].

Impedance spectroscopy data for porous LSCF electrodes on YSZ and Gd or Sm doped-CeO_2 (GDC or SDC) electrolytes have shown lower interfacial resistance than conventional LSM electrodes. The composite cathode, the proper addition of the ionic phase GDC/SDC to the cathode phase LSCF, results in the increase of triple phase boundaries (TPB) in the composite cathode and permits electrochemical reactions to occur within the electrode [3–5]. In addition, GDC in the cathode is considered to reduce the TEC without sacrificing the ionic conductivity. However, details concerning the electrochemical properties of the L58SCF–GDC composite cathodes are not reported.

In the present study we analyze the composite cathode performance of addition $Ce_{0.8}Gd_{0.2}O_{2-\delta}$ to $La_{0.58}Sr_{0.4}Co_{0.2}Fe_{0.8}O_{3-\delta}$. Impedance spectroscopy measurements were carried out at temperatures between 600 and 800 °C in order to analyze cathodic polarization resistance of the solid state half-cells. YSZ electrolytes were used in order to determine the feasibility of using the composite cathode with this standard electrolyte material.

2. Experimental

GDC was prepared by an oxalate coprecipitation route [7] with cerium nitrate hexahydrate ($Ce(NO_3)_3{\cdot}6H_2O$, 99.5%, Gansu Rare Earth Group) and gadolinium nitrate hexahydrate ($Gd(NO_3)_3{\cdot}6H_2O$, 99.5%, Gansu Rare Earth Group). The result-

* Corresponding author. Tel.: +86 451 86412153; fax: +86 451 86412153.
E-mail address: sunkn@hit.edu.cn (K. Sun).

0378-7753/$ – see front matter © 2007 Elsevier B.V. All rights reserved.
doi:10.1016/j.jpowsour.2007.03.040

ing precipitate was vacuum-filtered, and washed five times with water and ethanol, respectively, and then dried at 80 °C in an oven. The dry oxide powders were calcinated at 750 °C for 5 h.

L58SCF was synthesized by the citrate method [8] with these materials, $La(NO_3)_2{\cdot}6H_2O$ (99.5%, Gansu Rare Earth), $Sr(NO_3)_2$ (99.5%, Gansu Rare Earth), $Fe(NO_3)_3{\cdot}9H_2O$ (98.5%, Gansu Rare Earth), $Co(NO_3)_2{\cdot}6H_2O$ (99%, Gansu Rare Earth) and citric acid (99.5%, Tianjin Bodi). Mole ratio of citric acid to total metal cation content (abbreviated as C/M) is 1.8. The nitrates were weighed according to the nominal composition of $La_{0.58}Sr_{0.4}Co_{0.2}Fe_{0.8}O_3$ and then dissolved in a beaker of deionized water. After adding a designed amount of citric acid, small amounts of ammonia solution (content 25–28%, Tianjin Bodi) was dripped to adjust the pH of the precursor solution. The precursor solution was dehydrated at 80 °C to form a sol, followed by a further heating at 150 °C to yield a gel. The resulting gel was pulverized and calcinated at 750 °C for 2 h.

YSZ powders (40 nm, Tohso) were cold-pressed into pellets with the size of 13 mm in diameter and 0.7 mm in thickness, and then sintered at the temperatures 1500 °C for 5 h. The composite working electrodes (WE) L58SCF–GDC (L58SCF:GDC = 70:30, 60:40, 50:50, 40:60, wt.%; and hereafter are identified as L58SCF–GDC30–L58SCF–GDC60) was prepared by mixing $La_{0.58}Sr_{0.6}Co_{0.2}Fe_{0.8}O_{3-\delta}$ powder with $Gd_{0.2}Ce_{0.8}O_{2-\delta}$ powder using roll milling. The average particle size of the starting powders was 0.47 μm (d_{50}) for the L58SCF and 0.16 μm (d_{50}) for the GDC by Laser Particle Sizer (LS900, OMEC). L58SCF–GDC powder was then mixed with terpineol (solvent) and ethyl cellulose (binder) to form a cathode paste. The paste was applied on the one side of electrolyte using screen-printing method, which followed by sintering at 1000 °C for 2 h. Before coating, the YSZ substrates were roughed using 240 mesh SiC paper in order to improve adhesion between the cathode film and electrolyte substrate. The thickness of composite cathode was about 20 μm and the cathode area was about 0.25 cm^2.

The cross-section of the composite cathodes was polished using SiC 1000 mesh paper, and then was coated with gold to obtain conductive gold film. Morphology and component of the composition cathode were examined by a FEI SIRION scanning electron microscope (SEM). The compositions of the composition cathode were analyzed by Energy dispersive X-ray spectroscopy (EDS, LeicaS440). The phase of L58SCF–GDC40 composite cathode was examined with Rigaku D/max-ΠB X-ray diffractometer (XRD) using Cu Kα radiation.

Impedance measurements were carried out using a potentiostat/galvanostat (model PARSTAT® 2273, Princeton Applied Research). Three-electrode setup was used with the cathode as the working electrodes (WE). A commercial Pt paste (PC-Pt-7840, Sino-Platinum Metals) was applied to the edge of the same side of electrolyte as reference electrode (RE) and to the other side of electrolyte as the count electrode (CE), Fig. 1. The frequency range was 10 mHz to 10^5 Hz with a signal amplitude of 5 mV. Measurements were taken over a temperature range of 600–800 °C at air under open circuit potential. The impedance fitting analysis was controlled with software (Zsimpwin).

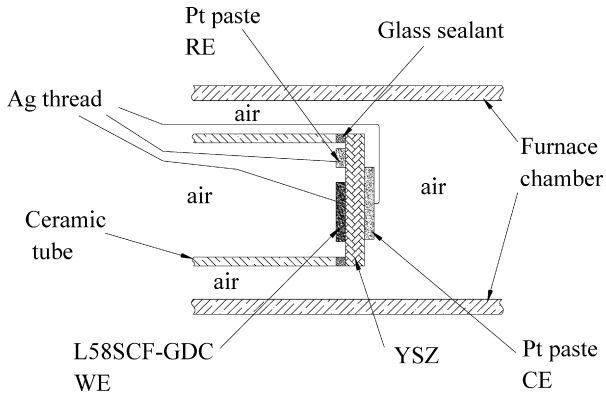

Fig. 1. Holder is for three-electrode SOFC for high temperature electrochemistry measurement.

3. Results and discussion

3.1. XRD and SEM of the L58SCF–GDC40 composite cathodes

Fig. 2 shows the XRD pattern of the L58SCF–GDC40 composite cathode. No resistive phases, either $La_2Zr_2O_7$ or $SrZrO_3$, are detected by X-ray diffraction for the L58SCF–GDC40 cathode on YSZ sintered at 1000 °C for 2 h. A well defined perovskite L58SCF oxide phase and GDC oxide phase can be seen from Fig. 2. However there are some extra peaks with small size in the XRD pattern. We find they belong to strontium iron oxide ($Sr_3Fe_2O_{6+\delta}$) by XRD phase analysis software. $Sr_3Fe_2O_{6+\delta}$ is a kind of the perovskite material related mixed ionic-electronic conductor, and not considered to be detrimental to the SOFC cathode [38,39]. Fig. 3(a–c) shows the SEM photographs of the cathode L58SCF–GDC40 and L58SCF, and sintered at 1000 °C for 2 h. It is confirmed in Fig. 3(a) that the GDC particles (bright phases in the image) are homogeneously dispersed in the L58SCF (dark phases). In Fig. 3(b and c), the particles of L58SCF–GDC40 are found to be continuous and to form the three-dimensional framework of the composite electrode. The particles of the L58SCF–GDC40 are well attached to each other and a large number of porosity (31%) in the film provides the gas a pathway for easier transport. The L58SCF retains a small particle size and the addition of the GDC extends a triple phase

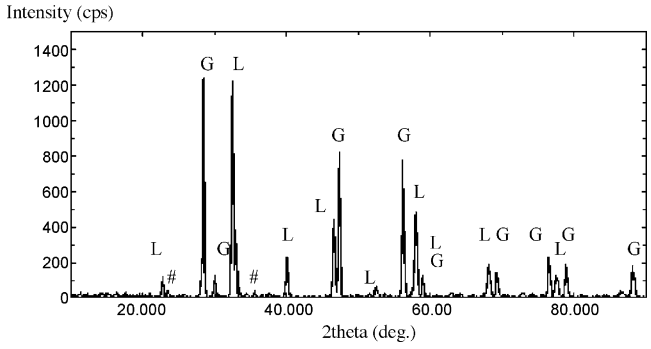

Fig. 2. XRD peaks of the L58SCF–GDC40 composite electrode, deposited on the YSZ disc, and heated at 1000 °C for 2 h. L: L58SCF; G: GDC; #: strontium iron oxide ($Sr_3Fe_2O_{6+\delta}$).

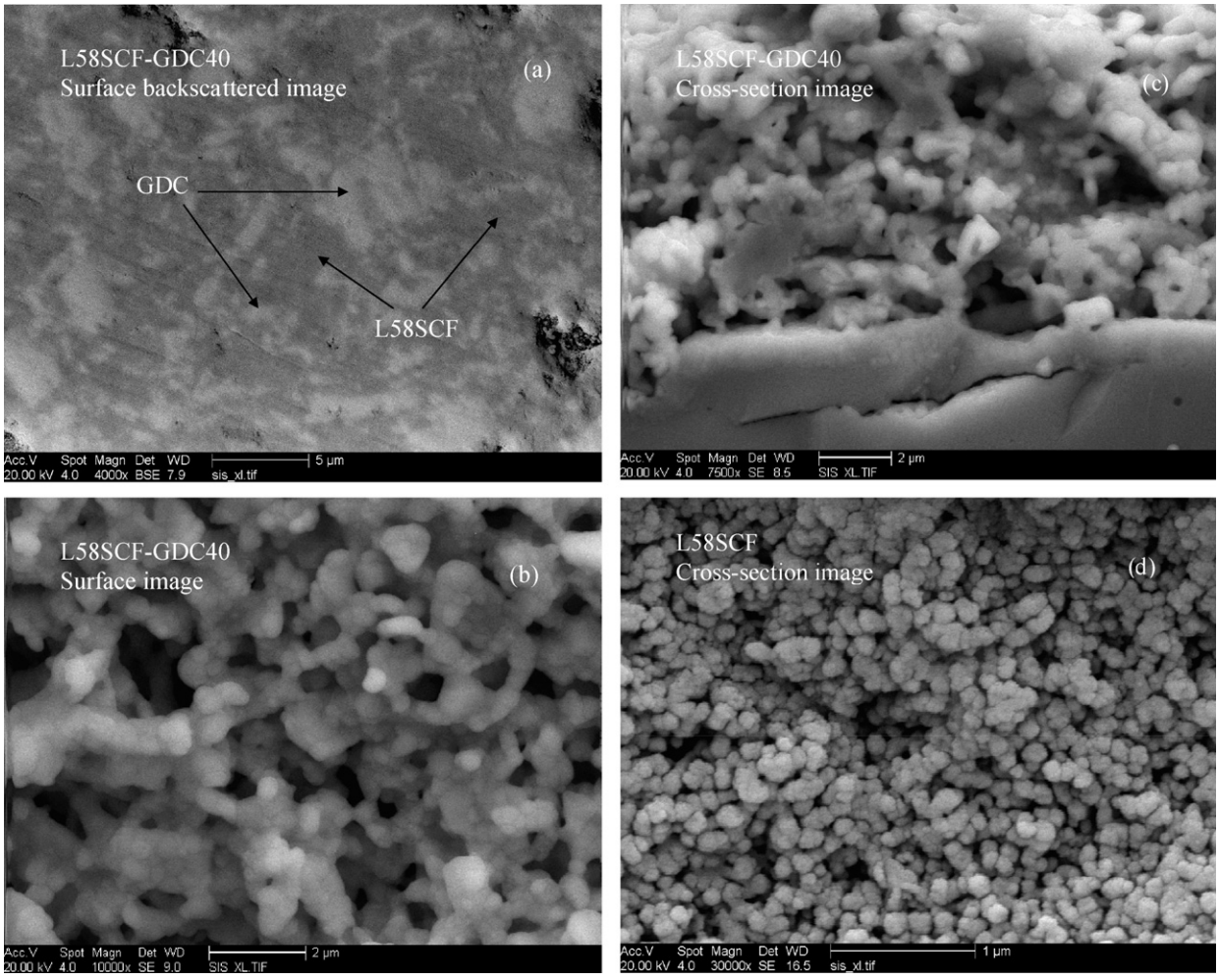

Fig. 3. SEM photograph showing cross-section of the L58SCF–GDC40 and the L58SCF cathode sintered at 1000 °C for 2 h. (a) Surface backscattered image of the L58SCF–GDC40, (b) surface image of the L58SCF–GDC40, (c) cross-section image of the L58SCF–GDC40 and (d) cross-section image of the L58SCF.

boundary length (TPBL). The EDS patterns in Fig. 4(a and b) corresponding to selected areas in Fig. 3(a) show the L58SCF and the GDC phases in the composite cathode, respectively. The combination of two materials with different rate-limiting processes may allow a "short circuiting" of the limiting steps of each. For example, the GDC may provide rapid mass transport, while the L58SCF may provide sites for efficient charge-transfer and surface exchange [9]. Nevertheless, it can be seen that the GDC particles are agglomerated slightly in the composite cathode in Fig. 3(a). The GDC particles are not sufficiently dispersed in the composite matrix during preparation. This means that it is still possible to further improve the electrochemical activity of the electrode.

3.2. Impedance analyses for the L58SCF–GDC and the L58SCF cathode

The intercept of the impedance arc with the real axis at high frequencies corresponds to the ohmic resistance of the cell, which includes the resistance of the electrolyte, the electrode–electrolyte interface and the lead wire, whereas the one at low frequencies relates to the total resistance of the cell.

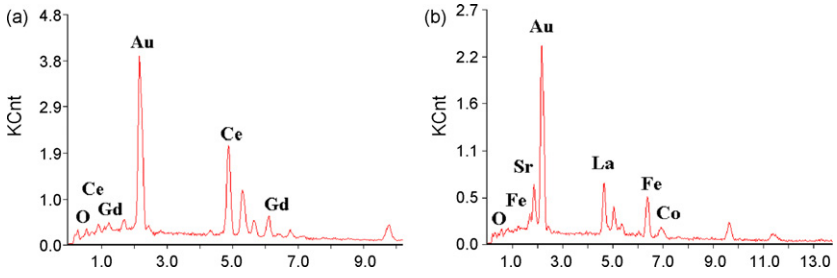

Fig. 4. (a and b) EDS patterns corresponding to selected areas in Fig. 3(a), energy unit of the horizontal axis is the keV.

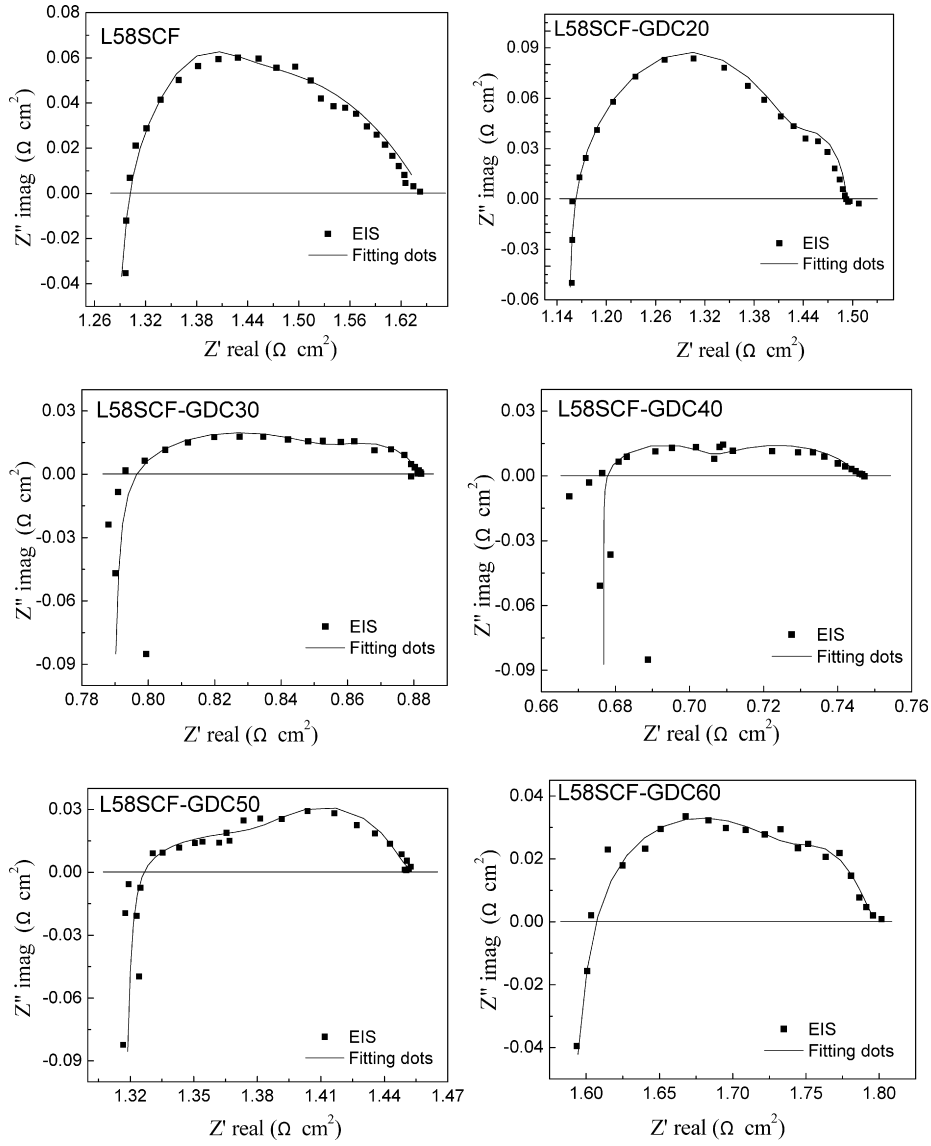

Fig. 5. Impedance spectra measured under open circuit condition at 800 °C in air for the L58SCF–GDC and the L58SCF cathodes.

In general, the interfacial polarization resistance [10,11] (R_p) can be given by subtracting the low frequency intercept from the high frequency intercept. Low polarization resistances from the electrode–electrolyte interfaces offer high catalytic activity [12,13].

Fig. 5 shows the impedance spectra for the L58SCF and different L58SCF–GDC composite cathodes sintered at 1000 °C for 2 h. When test temperature ≥650 °C, the induction can be observed in high frequency tail in Fig. 5. The size of the impedance arcs decreases with increasing X (X denotes GDC content, wt.%) from 20 to 40 wt.%. But the arcs increase, when $X > 40$ wt.%. When $X = 40$ wt.%, the impedance arc becomes smaller than other composition arcs. The impedance arc of the pure L58SCF cathode is a larger arc than that of the L58SCF–GDC40. The L58SCF–GDC40 depict the smallest cathode polarization resistance (0.07 Ω cm^2 at 800 °C) among all the cathodes (Table 1). The equivalent circuit of the impedance curves was the same as that in Fig. 6.

Fig. 6 shows the impedance spectra for the L58SCF–GDC40 cathode sintered at 1000 °C for 2 h and the equivalent circuit of the impedance curves. The observed separable two impedance arcs at low and high frequencies for the L58SCF–GDC40 show, however, that the oxygen reduction reaction is at least limited by two electrode processes during molecular oxygen reduction. The low frequency arc can be attributed to the diffusion pro-

Table 1
The sample cathodic polarization resistances at the test temperature 650–800 °C, sintering temperature 1000 °C (Ω cm^2)

T (°C)	1#	2#	3#	4#	5#	6#
650	2	2.44	3.31	0.52	1.27	1.94
700	0.745	1.18	0.53	0.22	0.61	0.79
750	0.345	0.57	0.17	0.11	0.25	0.4
800	0.21	0.33	0.09	0.07	0.12	0.2

1#: L58SCF; 2#: L58SCF–GDC20; 3#: L58SCF–GDC30; 4#: L58SCF–GDC40; 5#: L58SCF–GDC50; 6#: L58SCF–GDC60.

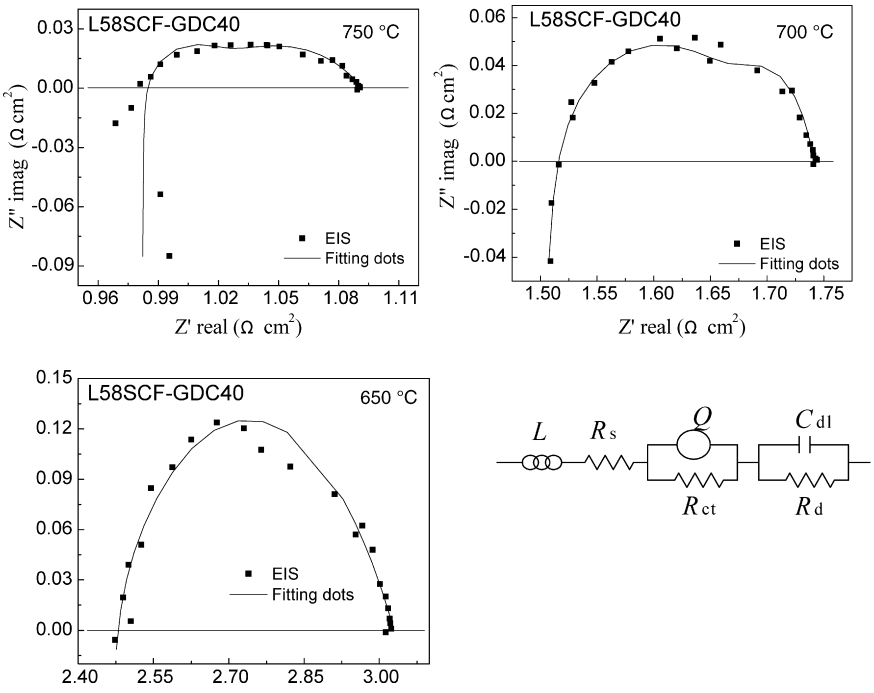

Fig. 6. Impedance spectra measured under open circuit condition in air for the L58SCF–GDC40 cathode. The equivalent circuit of the impedance curves for the L58SCF–GDC and the L58SCF cathodes.

cesses, which include adsorption–desorption of oxygen, oxygen diffusion at the gas–film interface and surface diffusion of intermediate oxygen species. The high frequency arc is probably associated with charge-transfer processes, which include oxide ion diffusion in the bulk of cathode and incorporation of oxygen ions from three-phase boundary into YSZ lattice [14,15]. For the L58SCF–GDC40, the high-frequency arc is larger than the low-frequency arc in the lower temperature, which indicates charge-transfer processes probably limit the electrode reaction in the lower temperature. With increasing temperature for the L58SCF–GDC40, the sizes of low-frequency arc are enlarged gradually, but also lower than that of the high-frequency arc, which typically indicates that the primary rate-limiting mechanism is related with charge-transfer processes [3]. These results emphasize the fact that under cathodic polarization the kinetic processes of the oxygen reduction are not only controlled by charge-transfer but also by adsorption–desorption and diffusion of oxygen. This is coherent with the fact that oxygen need to diffuse through the porous cathode, to adsorb on the L58SCF–GDC40 before being able to accept the electrons during the reduction and consequently oxygen ions are injected into the GDC particles that transport the ions to the cathode–electrolyte interface [16]. Hence, it is conceivable that the polarization resistance of the optimized composite electrode is decreased by extending TPBL, which results in much lower overpotential toward oxygen reduction, and by increasing the oxygen diffusion upon addition of an ionic conducting phase (GDC). Mizusaki et al. [17] studied the relationship between reaction kinetics and microstructures by the use of LSM as a cathode. They found that the limiting current not only depends on the electrode morphology along the three-phase boundary line but also on the internal cathode surface area, if a very limited internal surface area was provided for the cathode. They concluded that the surface diffusion processes also played a key role of oxygen reduction.

Impedance spectra of the L58SCF–GDC40 and the L58SCF in Fig. 5 depict the cathode polarization resistance of the L58SCF–GDC40 is smaller than that of the L58SCF (showed in Table 1) and suggest that the GDC in the cathode improved oxygen diffusion rates and charge-transfer rates of oxygen ions at the electrode–electrolyte interface [6]. It is apparent that the better performance of the L58SCF–GDC40 composite cathode than that of the pure L58SCF was from the enlarging of the electrochemical reaction zone. For efficient fuel cell operation, a value of $R_p < 1\ \Omega\,cm^2$ is desired [18]. In the present study, the L58SCF–GDC40 composite cathode displays the lower R_p of $0.07\ \Omega\,cm^2$ at 800 °C, $0.11\ \Omega\,cm^2$ at 750 °C and $0.22\ \Omega\,cm^2$ at 700 °C. Xia et al. [19] prepared the LSM–GDC (50:50 wt.%) composite cathode via a sol–gel process and found the polarization resistance of the composite cathode was $0.28\ \Omega\,cm^2$ at 700 °C. Murray and Barnett reported [20] the R_p of the LSM–GDC50 on the electrolyte GDC was $0.34\ \Omega\,cm^2$ at 750 °C. Leng et al. [21] reported that the LSM–GDC composite (GDC: 30 wt.%) cathode showed ≈13 times lower electrode polarization resistance (≈$0.60\ \Omega\,cm^2$ at 750 °C under open circuit) than that of pure LSM cathode (≈$8.19\ \Omega\,cm^2$ at 750 °C under open circuit) on YSZ electrolyte substrates. It is evident that the L58SCF–GDC40 composite cathode can be potential application on YSZ in intermediate/low-temperature SOFC.

It is known that the oxygen vacancies on the electrode surface provide the reaction site for the reduction of the molecular oxygen. The oxygen vacancies provide the pass way for the diffusion of the reduced oxygen ions [33,34]. Thus the oxide ion conductivity can be increased by the creation of more oxygen

Table 2
Inductance, charge transfer resistance, double layer capacitance, and exchange current density of the ORR at the L58SCF–GDC40 composite cathodes

T (°C)	L ($\times 10^{-7}$ H cm^2)	R_s (Ω cm^2)	Q (Ω^{-1} cm^{-2} s^n)	n	R_{ct} (Ω cm^2)	C_{dl} (F cm^{-2})	R_d (Ω cm^2)
650	0.81	2.481	0.05715	0.54	0.4502	0.00111	0.1015
700	1.164	1.514	0.01962	0.68	0.1661	0.145	0.0594
750	1.393	0.9849	0.3793	0.63	0.0730	0.00354	0.03318
800	1.40	0.6794	0.9939	0.64	0.0436	0.00791	0.02388

vacancies. The charge compensation mechanism in A-site deficient perovskites is the formation of the oxygen vacancies rather than $B^{3+} \rightarrow B^{4+}$ in the B-site [2]. Andreas et al. [6] reported A-site deficient perosvkite material L58SCF increased the ionic and electronic conductivity and oxide ion diffusivity, which can be explained by the larger number of the oxygen vacancies and electronic holes. The R_p of the L58SCF–GDC40, which is 0.11 Ω cm^2 at 750 °C, is higher than that of the LSCF–GDC in Ref. [3], which is 0.01 Ω cm^2 at 750 °C. Such a result is attributed to the weaker agglomeration of GDC particles in the L58SCF–GDC composite cathode (showed in Fig. 3(a)). Further optimization of the fabrication process for L58SCF–GDC composite cathode is required to minimize the agglomeration of the GDC particles in the L58SCF–GDC composite cathode. Jiang [37] used $Gd_{0.1}Ce_{0.9}(NO_3)_x$ to impregnate LSM cathode, his research showed that after ion impregnation with $Gd_{0.1}Ce_{0.9}(NO_3)_x$, very fine particles were formed around LSM particles and their particle size was in the range of 100–200 nm. $Ce_{0.9}Gd_{0.1}O_{2-\delta}$ particles were deposited on the LSM surface and at the electrode–electrolyte interface region. Thus the impregnation method will be an effective technique to solve the problem of agglomeration of the GDC particles in the L58SCF–GDC composite cathode in the next step work.

The oxygen reduction reaction at the L58SCF–GDC40 and the L58SCF on YSZ have been modeled using a equivalent circuit, LR(QR) (CR), as shown in Fig. 6. The electrochemical impedance spectroscopy (EIS) data (for L58SCF–GDC40) are fitted to the equivalent circuit shown in Table 2, with R_d/C_{dl} and R_{ct}/Q units in series with a resistor (R_s) and an inductor (L). A high-frequency inductive component coming from the measuring system is visible at temperatures above 650 °C. The series resistance, R_s, corresponds to the overall ohmic resistance including of the electrolyte resistance between the WE and the RE, the contact resistance at the electrode–electrolyte interface and the resistance of the lead wires. The resistance R_d may relate to the oxygen adsorption–desorption on the electrode particle surface and surface diffusion of intermediate oxygen species. The resistance R_{ct} can be attributed to the polarization during charge-transfer [3,25]. The capacitance C_{dl} as the double-layer capacitance, is contributed to the interfacial capacitance at the WE and YSZ electrolyte. Q is the constant phase element, n is the frequency power [22]. The R_d is attributed by the oxygen adsorption–desorption and the diffusion of the oxygen ions. The oxygen vacancies concentration of the cathode material should play an important role on the change of the R_d value. When the current passes, the reduction of the molecular oxygen-to-oxygen ions on the triple phase boundary can be greatly enhanced, and the oxygen-ion concentration gradient around the TPB region is then being increased. Therefore, the diffusivity of the oxygen ions can be improved. This ionic conductivity improvement enhances the diffusion of the oxygen ions, which are reduced on the electrode surface from the electrode surface to the TPB. This phenomenon can be seen as the extending of the TPB [25,35,36].

With increasing temperature, both R_s and R_{ct} are observed to decrease significantly, as shown in Table 2. It is found that the decreasing size of the arc on the high frequencies ($R_{ct} - Q$) is relatively larger than that on the low frequencies with increasing temperature. This result interprets that abilities of charge-transfer on the electrode surface are enhanced for the L58SCF–GDC composite cathode in the high temperature.

Dusastre's paper [9] showed that the composite cathode $La_{0.6}Sr_{0.4}Co_{0.2}Fe_{0.8}O_{3-\delta}/Ce_{0.9}Gd_{0.1}O_{2-\delta}$ containing 30% in weight (36% in volume) $Ce_{0.9}Gd_{0.1}O_{2-\delta}$ exhibited the lowest interfacial resistance or the highest catalytic activity for oxygen reduction, which classified this composite cathode as a promising material for intermediate temperature SOFC based on $Ce_{0.9}Gd_{0.1}O_{2-\delta}$ electrolytes. Ionic charge-transfer reactions at mixed conducting electrode surfaces may be driven by vacancy concentration variations in the electrode rather than by electrostatic fields and can yield a diode-like behavior [23].

Penetration depth studied by Adler et al. [14] have indicated that, for the mixed-conducting oxides with an average particle size of 1 μm, the electrode reaction zone extended up to 10 μm from the electrode–electrolyte interface. The large reaction surface of these composite cathodes, especially the L58SCF–GDC40, might be generated from the effective suppressing of the sintering and growth of the L58SCF particles by the GDC particles during the cathode firing [5,24].

3.3. Activation energies of the cathode polarization for the L58SCF–GDC

Activation energies (E_a) of the cathode polarization are derived from the Arrhenius equation (Eq. (1)). The slope of the $\log \delta T$ versus $1000/T$ data is the activation energy of the L58SCF–GDC composite cathodes (in Table 3). It is lower than prior studies of $La_{0.6}Sr_{0.4}Co_{0.2}Fe_{0.8}O_{3-\delta}$ cathodes where activation energies of ≈1.5 eV were reported [9,26] and pure GDC phase where activation energies of ≈0.9 eV [9]. The main reason might be that higher oxygen defect concentration, which

Table 3
The activation energies (E_a) of the L58SCF–GDC composite cathodes (eV)

	1#	2#	3#	4#	5#	6#
E_a	1.24	1.10	1.28	1.10	1.35	1.31

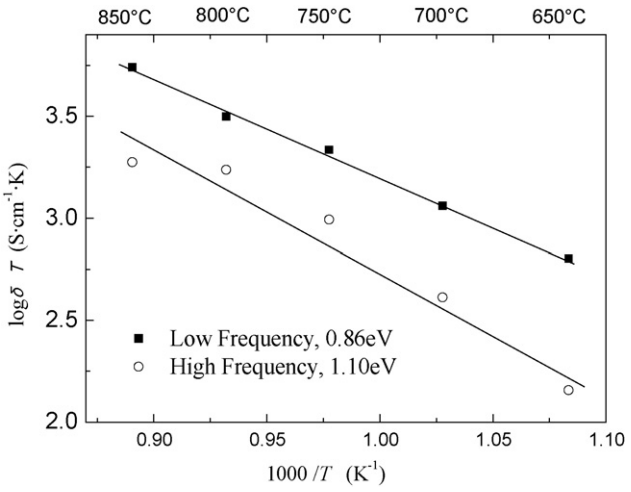

Fig. 7. Arrhenius plots of the conductivity as a function of temperatures for the low- and high-frequency arcs for the L58SCF–GDC40 composite cathode, sintered at 1000 °C for 2 h.

increases the oxygen vacancy concentration, is in the A-site deficient composite cathode L58SCF–GDC [6].

$$\delta = A_0 T^{-1} \exp(-E_a K^{-1} T^{-1}) \quad (1)$$

where A_0 is the pre-exponential factor, T the absolute temperature, E_a the activation energy for small polaron hopping, and K is the Boltzmann constant.

The activation energy values typically indicate that the oxygen reduction reaction (ORR) mechanism is related with the charge-transfer processes and the diffusion processes. Activation energy (L58SCF–GDC40, in Fig. 7) value of high-frequency arc (1.10 eV) is lower than that of low-frequency arc (0.86 eV). As mention above, the low frequency arc can be attributed to the diffusion processes, the high frequency arc are probably associated with the charge-transfer processes. Fig. 7 shows that the charge-transfer in the electrode is more difficult than the diffusion and adsorption–desorption of oxygen at the gas–electrode interface. Murray and Barnett [20] investigated the performance of LSM–GDC50 composite cathode on YSZ electrolyte. The activation energy values for the low- and high-frequency arcs for LSM–GDC50 were 1.26 and 0.92 eV, respectively. The comparative result indicates that diffusion and adsorption–desorption of oxygen and charge-transfer processes in the L58SCF–GDC40 cathode can be easier than that in the LSM–GDC50.

3.4. Determination the exchange current density (i_0) of the L58SCF–GDC40

The exchange current, i_0, the intrinsic oxygen reduction reaction rate, can be obtained electrochemically using AC impedance spectroscopy. The i_0 values obtained from the AC impedance measurements at all temperatures are tabulated in Table 4. For a simple system, i_0 can be obtained from the diameter (charge-transfer resistance, R_{ct}) of the Nyquist plot is calculated using Eq. (2). Eq. (2) is derived from the low-field approximation to the Bulter–Volmer equation [27–30].

$$i_0 = RT\upsilon(nFR_{ct})^{-1} \quad (2)$$

Here n is the total number of electrons passed in the reaction, υ reflects the number of times the rate-determining step occurs for one occurrence of the full reaction, F the Faraday constant, R the gas constant. For the ORR, n and υ are assumed to be 4 and 1, respectively (as the total number of electrons passed per molecule of oxygen reduced is 4 and the rate limiting step would likely have a stoichiometry of 1 for the oxygen reduction reaction) [31].

Values for i_0 obtained from Eq. (2) are given in Table 4. It is observed that the i_0 increases from 9.79 to 529 mA cm^{-2} by increasing the cell temperature from 600 to 800 °C. Table 4 also shows that the i_0 of the L58SCF–GDC40 in all the test temperatures are larger than that of the LSM–YSZ composite cathode. These results suggest that the electrocatalytic activity of the L58SCF–GDC40 is higher than that of the LSM–YSZ. The higher electrocatalytic activity can arise from a number of sources. First, the L58SCF will have a significantly larger active surface area and higher porosity than the LSM, although it may have been anticipated that the composite nature of the latter material would have offset these particle size (surface area) differences. Secondly, the ORR kinetics at the L58SCF–GDC interface may be inherently higher than that at the LSM–YSZ interface. However, most significantly, these results suggest strongly that the L58SCF–GDC, which is known to be a mixed ionic-electronic conductor (MIEC), is active even in regions well away from the underlying YSZ electrolyte [32]. In other words, the ORR is occurring at the air–L58SCF interface, as well as at the air–L58SCF–GDC triple phase boundary, while in the case of LSM–YSZ, only the triple phase boundaries are active. These results clearly show the impressive advantages of using the L58SCF–GDC, the MIEC materials, as electrodes in solid oxide fuel cells [31].

Table 4
Exchange current density of the ORR at the composite cathodes

T (°C)	i_0 (EIS) (mA cm^{-2})				
	L58SCF–GDC40	LSCF [31]	LSM–YSZ [31]	LSM–YSZ [16]	LSM–YSZ [28]
600	9.79	13	0.45		2.4
650	44.1			(660 °C) 13	
700	126	65	5.8	(690 °C) 24	31
750	301			69	
800	529			(810 °C) 194	230

Next steps for this study are to study the long-term stability of the L58SCF–GDC40 performance on YSZ under SOFC operating conditions.

4. Conclusion

The composite electrodes with the GDC added to A-site deficient perosvkite material L58SCF are investigated by AC impedance spectroscopy. The GDC in the cathode improve oxygen diffusion rates and charge-transfer rates of oxygen ions at the electrode–electrolyte interface and enlarge the electrochemical reaction zone in the composite.

The polarization resistances of the L58SCF–GDC40 (0.07 $\Omega\,cm^2$ at 800 °C, 0.11 $\Omega\,cm^2$ at 750 °C and 0.22 $\Omega\,cm^2$ at 700 °C) are smaller than that of the L58SCF and other composite cathodes. It is evident that the L58SCF–GDC40 can be potential applications cathode on YSZ in intermediate/low-temperature solid oxide fuel cells.

Activation energy values of the L58SCF–GDC40 calculated for the low- and high-frequency arcs are 0.86 and 1.10 eV, respectively.

The analysis of the EIS data of L58SCF–GDC40 suggests that charge-transfer process can be the key process in the cathodic reaction. The exchange current densities of the composite cathode are determined from the charge-transfer resistance obtained from the EIS experiments by the low-field approximation to the Bulter–Volmer equation. The exchange current densities of the L58SCF–GDC40 are 126 mA cm^{-2} at 700 °C, 301 mA cm^{-2} at 750 °C and 529 mA cm^{-2} at 800 °C.

Acknowledgment

This project is financially supported by the National Natural Science Foundation of China (No. 90510006).

References

[1] B.C.H. Steele, J.-M. Bae, Solid State Ionics 106 (1998) 255–261.
[2] G.Ch. Kostogloudis, Ch. Ftikos, Solid State Ionics 126 (1999) 143–151.
[3] E.P. Murray, M.J. Sever, S.A. Barnett, Solid State Ionics 148 (2002) 27–34.
[4] S.B. Adler, Chem. Rev. 104 (2004) 4791–4843.
[5] H.J. Hwang, J.-W. Moonb, S. Lee, E.A. Lee, J. Power Sources 145 (2005) 243–248.
[6] A. Mai, A.C. Vincent Haanappel Sven Uhlenbruck, F. Tietz, D. Stöver, Solid State Ionics 176 (2005) 1341–1350.
[7] K. Higashi, K. Sonoda, H. Ono, S. Sameshima, Y. Hirata, J. Mater. Res. 14 (1999) 957–967.
[8] Q. Xu, D.-P. Huang, W. Chen, J.-H. Lee, H. Wang, R.-Z. Yuan, Scripta Mater. 50 (2004) 165–170.
[9] V. Dusastre, J.A. Kilner, Solid State Ionics 126 (1999) 163–174.
[10] A. Petric, P. Huang, F. Tietz, Solid State Ionics 135 (2000) 719–725.
[11] H. Ullmann, N. Trofimenko, F. Tietz, D. Stöver, A. Ahmad-Khanlou, Solid State Ionics 138 (2000) 79–90.
[12] Y. Ji, J. Liu, T. He, J. Wang, W. Su, J. Alloys Compd. 389 (2005) 317–322.
[13] X.D. Zhu, K.N. Sun, N.Q. Zhang, X.B. Chen, L.J. Wu, D.C. Jia, Electrochem. Commun. 9 (2007) 431–435.
[14] S.B. Adler, J.A. Lane, B.C.H. Steele, J. Electrochem. Soc. 143 (1996) 3554–3564.
[15] X.J. Chen, S.H. Chan, K.A. Khor, Electrochim. Acta 49 (2004) 1851–1861.
[16] M.P. Carpanese, A. Barbucci, G. Cerisola, M. Viviani, Impedance Contributions Online 2 (2004) P7-1–P7-8. http://accessimpedance.iusi.bas.bg.
[17] J. Mizusaki, H. Tagawa, K. Tsuneyshi, A. Sawata, J. Electrochem. Soc. 138 (1991) 1867–1873.
[18] F.H. Van Heuveln, H.J.M. Bouwmeester, F.P.F. van Berkel, J. Electrochem. Soc. 144 (1997) 126–133.
[19] C.R. Xia, Y.L. Zhang, M.L. Liu, Electrochem. Solid State Lett. 6 (2003) A290–A292.
[20] E.P. Murray, S.A. Barnett, Solid State Ionics 143 (2001) 265–273.
[21] Y.J. Leng, S.H. Chan, K.A. Khor, S.P. Jiang, J. Solid State Electrochem. 10 (2006) 339–347.
[22] H.-K. Lee, Mater. Chem. Phys. 77 (2003) 639–646.
[23] J. Fleig, Chem. Chem. Phys. 7 (2005) 2027–2037.
[24] Z. Bi, M. Cheng, Y. Dong, H. Wu, Y. She, B. Yi, Solid State Ionics 176 (2005) 655–661.
[25] H.C. Yu, F. Zhao, A.V. Virkar, K.Z. Fung, J. Power Sources 152 (2005) 22–26.
[26] D. Waller, J.A. Lane, J.A. Kilner, B.C.H. Steele, Solid State Ionics 86–88 (1996) 767–772.
[27] Z. Shao, M. Sossina, Haile, Lett. Nat. 431 (2004) 170–173.
[28] A.C. Co, S.J. Xia, V.I. Birss, J. Eletrochem. Soc. 152 (2005) A570–A576.
[29] W. Franks, I. Schenker, P. Schmutz, A. Hierlemann, IEEE Trans. Biomed. Eng. 52 (2005) 1295–1302.
[30] Y. Matsuzaki, I. Yasuda, Solid State Ionics 126 (1999) 307–313.
[31] J. Liu, A.C. Co, S. Paulson, V.I. Birss, Solid State Ionics 177 (2006) 377–387.
[32] J. Liu, S.A. Barnett, Solid State Ionics 158 (2003) 11–16.
[33] T. Ishihara, T. Kudo, H. Matsuda, Y. Takita, J. Electrochem. Soc. 142 (1995) 1519–1524.
[34] S. Kim, S. Wang, X. Chen, Y.L. Yang, N. Wu, A. Ignatiev, A.J. Jacobson, B. Abeles, J. Electrochem. Soc. 147 (2000) 2398–2406.
[35] T. Horita, K. Yamaji, N. Sakai, H. Yokokawa, A. Weber, E. Iver-Tiffee, J. Electrochem. Soc. 148 (2001) A456–A462.
[36] S.P. Jiang, J.G. Love, J.P. Zhang, M. Hoang, Y. Ramprakash, A.E. Hughes, S.P.S. Badwal, Solid State Ionics 121 (1999) 1–10.
[37] S.P. Jiang, Mater. Sci. Eng. A 418 (2006) 199–210.
[38] L. Mogni, J. Fouletier, F. Prado, A. Caneiro, J. Solid State Chem. 178 (2005) 2715–2723.
[39] M.V. Patrakeev, I.A. Leonidov, V.L. Kozhevnikov, V.V. Kharton, Solid State Sci. 6 (2004) 907–913.